International Journal of Pharmaceutics 423 (2012) 509–515

Contents lists available at SciVerse ScienceDirect

International Journal of Pharmaceutics

journal homepage: www.elsevier.com/locate/ijpharm

Pharmaceutical Nanotechnology

Cancer therapy improvement with mesoporous silica nanoparticles combining targeting, drug delivery and PDT

Magali Gary-Bobo[b], Ouahiba Hocine[a], David Brevet[a], Marie Maynadier[b], Laurence Raehm[a], Sébastien Richeter[a], Virginie Charasson[b], Bernard Loock[c,d], Alain Morère[e,*], Philippe Maillard[c,d], Marcel Garcia[b,*], Jean-Olivier Durand[a,*]

[a] Institut Charles Gerhardt Montpellier, UMR 5253 CNRS-UM2-ENSCM-UM1, CC1701 Equipe Chimie Moléculaire et Organisation du Solide, Place Eugène Bataillon, 34095 Montpellier Cedex 05, France
[b] Institut des Biomolécules Max Mousseron, Faculté de Pharmacie, 34093, Montpellier, France
[c] UMR 176 CNRS/Institut Curie, Institut Curie, Bât 110-112, Université Paris-Sud, F-91405 Orsay, France
[d] Institut Curie, Section de Recherches, Centre Universitaire, Université Paris-Sud, F-91405 Orsay, France
[e] UMR 5247 CNRS-UM2 et UM1 - Institut des Biomolécules Max Mousseron, Ecole Nationale Supérieure de Chimie de Montpellier, 8 rue de l'Ecole Normale, 34296 Montpellier, France

ARTICLE INFO

Article history:
Received 21 February 2011
Received in revised form
28 November 2011
Accepted 29 November 2011
Available online 8 December 2011

Keywords:
Mesoporous
Silica
Nanoparticles
Photodynamic therapy
Targeting
Drug delivery
Carbohydrates

ABSTRACT

The synthesis of Mesoporous Silica Nanoparticles (MSN) covalently encapsulating fluoresceine or a photosensitizer, functionalized with galactose on the surface is described. Confocal microscopy experiments demonstrated that the uptake of galactose-functionalized MSN by colorectal cancer cells was mediated by galactose receptors leading to the accumulation of the nanoparticles in the endosomal and lysosomal compartments. The MSN functionalized with a photosensitizer and galactose were loaded with the anticancer drug camptothecin. Those MSN combining drug delivery and photodynamic therapy were tested on three cancer cell lines and showed a dramatic enhancement of cancer cell death compared to separate treatments.

1. Introduction

The development of Mesoporous Silica Nanoparticles (MSN) for biological applications has grown a lot the last decade (Coti et al., 2009; Liong et al., 2009; Rosenholm et al., 2010a; Slowing et al., 2007, 2008; Trewyn et al., 2007a,b). Due to their interesting properties (Rosenholm et al., 2010c; Slowing et al., 2010) (monodispersity, high specific surface area, tunable pore size and diameter, versatile functionalization), MSN were designed for diagnostic [fluorescence imaging (Lee et al., 2009; Lin et al., 2005) and/or MRI (Hsiao et al., 2008; Liong et al., 2008; Liu et al., 2008; Na and Hyeon, 2009; Taylor et al., 2008; Wu et al., 2007)], and for therapy [drug delivery (Coti et al., 2009; Vivero-Escoto et al., 2010) or photodynamic therapy (Cheng et al., 2009, 2010; Couleaud et al., 2010; Guo et al., 2010; Kim et al., 2009; Tu et al., 2009; Yang et al., 2010)]. Many different drugs such as paclitaxel (Lu et al., 2007a; Vivero-Escoto et al., 2009), camptothecin (Lu et al., 2007b, 2008), doxorubicin (Lebold et al., 2009; Lee et al., 2010), methotrexate (Rosenholm et al., 2010b), colchicine (Cauda et al., 2010), chlorambucil (Lin et al., 2010), cysteine (Mortera et al., 2009), telmisartan (Zhang et al., 2010), have been successfully loaded in MSN or covalently grafted at MSN. Anti-cancer drugs vectorized using MSN efficiently led to the death of cancer cells. Furthermore, camptothecin-loaded MSN were shown to be very efficient in inducing tumor regression in vivo (Lu et al., 2010). To overcome drug resistances which are major obstacles in cancer therapy, co-delivery of si-RNA and doxorubicin has been demonstrated to enhance the efficiency of chemotherapy in vitro (Chen et al., 2009; Meng et al., 2010). To further improve the efficiency of MSN, targeting of cancer cells with biomolecules (Brevet et al., 2009; Cheng et al., 2010; Gary-Bobo et al., 2011; Lebret et al., 2010, 2008; Liong et al., 2008; Rosenholm et al., 2009) or antibodies (Tsai et al., 2009) anchored on the MSN surface has been carried out. The penetration of the MSN inside

* Corresponding authors. Tel.: +33 4 67 14 45 01; fax: +33 4 67 14 38 52.
E-mail addresses: morere@univ-montp2.fr (A. Morère), m.garcia@inserm.fr (M. Garcia), durand@univ-montp2.fr (J.-O. Durand).

0378-5173/$ – see front matter © 2011 Elsevier B.V. All rights reserved.
doi:10.1016/j.ijpharm.2011.11.045

cells is thus more efficient due to an active endocytosis pathway involving specific over-expressed receptors at the cell surface. In this work, we have examined the potential of MSN having pores loaded with camptothecin, possessing a photosensitizer (PS) in the walls, and functionalized with galactose on the surface. Indeed, the alkaloid camptothecin is an anticancer agent that targets a nuclear enzyme: DNA topoisomerase I which plays a crucial role in the removal of the DNA supercoiling associated with DNA replication and transcription (Gallo et al., 1971; Li et al., 1972). This very promising active principle entered in phase I and II clinical trials, but had to be abandoned following the onset of toxic manifestations due to recyclisation in acidic solutions of the sodium salt originally used, leading to local overexposure (Gottlieb et al., 1970). Nevertheless, MSN now allows the use of this poorly water soluble drug (Lu et al., 2007b, 2008). Therefore, in this study, we have examined MSN combining camptothecin delivery, photodynamic therapy (PDT) and cell targeting with galactose in order to further enhance the anti-cancer activity of the MSN. The drug delivery potential of these targeted MSN was tested on human cell lines of colorectal (HCT-116), pancreatic (Capan-1) and breast cancer (MDA-MB-231). We show here that treatment with MSN combining camptothecin delivery and PDT led to a dramatic enhancement of cancer cell death compared to separate treatments.

2. Materials and methods

All solvents used were reagent grade. The following reagents have been abbreviated, dimethylformamide (DMF), triethylamine (Et_3N), diisopropylethylamine (DIPEA). aminopropyltriethoxysilane (APTS), cetyltrimethylammonium bromide (CTAB) tetraethoxysilane (TEOS), fluorescein isothiocyanate (FITC). DMF was distilled under slow argon flow and kept over 4 Å sieves. Column chromatography was performed with the indicated solvents using E. Merck silica gel 60 (particle size 0.035–0.070 mm). Yields refer to chromatographically and spectroscopically pure compounds. ^{1}H NMR spectra were recorded on a Bruker AC-300 spectrometer at ambient temperature using an internal deuterium lock. Chemical shift values are given in ppm relative to tetramethyl silane (TMS). Acidic impurities in $CDCl_3$ were removed by treatment with anhydrous K_2CO_3. Quantitative UV–visible spectra were obtained using a Perkin-Elmer spectrometer (molar extinction coefficient values are given in L mmol^{-1} cm^{-1}). Transmission Electron Microscopy (TEM) measurements were carried out with a JEOL 1200 EXII microscope at 100 kV. Dynamic Light Scattering (DLS) experiments were run using a Cordouan Vasco 135 apparatus, with a 75 mW laser source operating at 658 nm. Specific surface areas were determined by Brunauer–Emmett–Teller (BET) method on a Micromeritics triStar analyser (using 75 points and starting from 0.01 as value for the relative pressure) and the average pore diameters were calculated by the BJH method.

2.1. Synthesis of galactose derivatives

2.1.1. 1-p-Aminophenyl-α-D-galactopyranoside

1-*p*-Nitrophenyl-α-D-galactopyranoside (1 g, 3.32 mmol) was dissolved in 125 mL of MeOH under argon atmosphere. To this solution was added 500 mg of Pd/C. The atmosphere was removed and changed to H_2 pressure. The solution was stirred for 2 h, filtered and evaporated to give a white powder in quantitative yield.

^{1}H NMR (200 MHz, DMSO) δ 3.15 (s, 1H), 3.26–3.68 (m, 6H), 4.67 (s, 2H), 5.07 (s, 1H), 6.48 (d, J = 12.9 Hz, 2H), 6.78 (d, J = 12.9 Hz, 2H).

^{13}C NMR (50 MHz, DMSO) δ 61.24, 69.12, 69.54, 70.40, 72.62, 100.75, 115.45, 119.70, 144.53, 149.35.

2.1.2. p-[N-(2-Ethoxy-3,4-dioxocyclobut-1-enyl)amino]phenyl-α-D-galactopyranoside

1-*p*-Aminophenyl-α-D-galactopyranoside (250 mg, 0.092 mmol) was dissolved in a 5/3 solution of ethanol/water (8 mL), and 3,4-diethoxy-3-cyclobutene-1,2-dione (150 μL, 1.1 equiv.) was dissolved in the same solution. The two solutions were mixed and stirred under argon for 20 h. Concentration followed by flash chromatography in AcOEt/MeOH (9:1, v/v) gave the galactopyranoside derivative (364 mg, 47%).

^{1}H NMR (200 MHz, DMSO) δ 1.13 (t, J = 7.05 Hz, 3H), 3.49 (m, 2H), 3.69 (m, 4H), 4.72 (m, 6H), 5.33 (s, 1H), 7.05 (d, J = 7.7 Hz, 2H), 7.25 (d, J = 7.9 Hz, 2H), 10.66 (s, 1H).

^{13}C NMR (50 MHz, DMSO) δ 16.50, 61.16, 68.85, 69.41, 70.21, 73.11, 99.49, 118.39, 121.96, 128.48, 132.93, 155.04, 170.29, 184.17.

2.2. Synthesis of MSN

MSN-FITC, *MSN-FITC-NH$_2$*, were already synthesized and described in ref Hocine et al. (2010).

2.2.1. MSN-FITC-gal

68 mg of *MSN-FITC-NH$_2$* were put in suspension in 5 mL EtOH. 4 mg (0.101 μmol) of *p*-[*N*-(2-Ethoxy-3,4-dioxocyclobut-1-enyl)amino]phenyl-α-D-galactopyranoside were dissolved in 5 mL EtOH/H_2O (1/1, v/v). This solution was added dropwise to the suspension of MSN. 500 μL of triethylamine (Et_3N) were added and the suspension was stirred for 18 h. After centrifugation (10 min, 20,000 rpm), nanoparticles were washed with water (3 cycles), then with EtOH twice. They were dried under vacuum.

2.2.2. MSN-PS

10 mg (5.44 μmol) of 5-*p*-aminophenyl-10,15,20-*p*-sulfonatophenyl-porphyrin were dissolved in 1.5 mL of ethanol; 13.57 μL (5 equiv.) of isocyanatopropyltriethoxysilane and 7.52 μL (4 equiv.) of DIPEA were added. The reaction was stirred at room temperature for 12 h. 646 mg (1.8 mmol) of CTAB were dissolved in 40 mL of 0.2 M NaOH at 25 °C. The silylated porphyrin was added to this mixture. After 5 min, 3.5 mL (15.7 mmol) of TEOS were added dropwise. After 40 s, 260 mL of deionised water were added to the mixture. The reaction was stirred for 6 min at 25 °C then rapidly neutralized to pH 7 by addition of 0.2 M HCl. Nanoparticles were obtained after centrifugation (10 min, 20,000 rpm), put in suspension in ethanol under ultrasounds and then centrifuged. CTAB was extracted with 50 mL of solution of EtOH/HCl 12 N (4/1, v/v) for 2 h at 60 °C. After centrifugation, the extraction procedure was repeated two times, and then nanoparticles were put in suspension in water and centrifuged, until neutral pH (m = 744 mg). Specific surface area (728 m^2 g^{-1}), volume of pores (0.50 cm^3 g^{-1}) and pores diameter (2.76 nm). Dynamic light scattering (DLS) showed a hydrodynamic diameter of 245 nm. Titration (UV–Vis) gave 9.76 μmol of PS per gram of *MSN-PS*.

2.2.3. MSN-PS-NH$_2$

200 mg of *MSN-PS* were put in suspension in 5 mL H_2O. 313 μL of APTS was diluted in 1.5 mL of EtOH. This solution was added to the nanoparticles suspension. The pH was adjusted to 7 by addition of 0.2 M HCl (4.5 mL). The reaction was stirred at RT for 20 h. Nanoparticles were centrifuged (10 min, 20,000 rpm) and washed with EtOH and dried under vacuum (m = 200 mg). Microanalysis: % C: 6.22; % H: 4.67; % N: 1.72. Loading of APTS: 1.22 mmol g^{-1}. Specific surface area (402 m^2 g^{-1}), volume of pores (0.23 cm^3 g^{-1}) and pores diameter (2.26 nm). D_{DLS} = 277 nm.

2.2.4. MSN-PS-gal

100 mg of *MSN-PS-NH$_2$* were put in suspension in 7.5 mL EtOH. 35 mg (0.88 μmol) of *p*-[*N*-(2-Ethoxy-3,4-dioxycyclobut

-1-enyl)amino]phenyl-α-D-galactopyranoside were dissolved in 5 mL EtOH/H_2O (1/1, v/v). This solution was added dropwise to the suspension of NP. 750 μL of Et_3N were added and the suspension was stirred for 18 h. After centrifugation (10 min, 20,000 rpm), nanoparticles were washed with water (3 cycles), then with EtOH twice. They were dried under vacuum. D_{DLS} = 313 nm.

2.2.5. MSN-PS-gal-CPT

25 mg of *MSN-PS-gal* were suspended and stirred in a solution of camptothecin (2.5 mg) in 1.5 mL of DMSO overnight. After centrifugation (10 min, 25,000 rpm) nanoparticles were washed with water, centrifuged (2 cycles) and dried under vacuum.

Titration (UV–vis) gave 7.11 μmol g^{-1} of camptothecin loaded in the MSN.

2.3. Cell culture conditions

Human colorectal (HCT-116), pancreatic (Capan-1) and breast (MDA-MB-231) cancer cell lines were purchased from ATCC (American Type Culture Collection, Manassas, VA). All cell types were allowed to grow in humidified atmosphere at 37 °C under 5% CO_2. Capan-1 human pancreatic and MDA-MB-231 human breast cancer cells were cultured in Dulbecco's Modified Eagle's Medium (DMEM) supplemented with 10% fetal bovine serum (FBS), phenol red, glutamine and 50 μg mL^{-1} gentamycin. HCT-116 human colorectal cancer cells were routinely maintained in Mc Coy's 5A medium, supplemented with 10% FBS, penicillin 100 U mL^{-1} and streptomycin 100 μg mL^{-1}.

2.4. Cytotoxicity assay for drug delivery

For the experiments, cancer cells were seeded into 96-well plates at 2×10^4 cells per well in 100 μL culture medium and allowed to grow for 24 h. Then cells were incubated at different times with or without 20 μg mL^{-1} of MSN. After incubation with MSN, cells were washed, maintained in fresh culture medium and two day after, a 3-(4,5-dimethylthiazol-2-yl)-2,5-diphenyltetrazolium bromide (MTT) assay was performed to evaluate the cytotoxicity of MSN. Briefly, cells were incubated in the presence of 0.5 mg mL^{-1} MTT for 4 h to determine mitochondrial enzyme activity. Then MTT precipitates were dissolved in 150 μL EtOH/DMSO (1:1, v/v) solution and absorbance was read at 540 nm.

2.5. Phototoxicity assay

Cancer cells were seeded into 96-well plates at 2×10^4 cells per well in 100 μL culture medium and allowed to grow for 24 h. Then cells were incubated for 24 h with or without 20 μg mL^{-1} of MSN. After incubation, cells were washed twice, maintain in fresh culture medium and then submitted or not to laser irradiation (630–680 nm; 6 mW cm^{-2}, 14 J cm^{-2}) for 40 min. Two days after irradiation, a MTT assay was performed to evaluate the cytotoxicity of MSN.

2.6. Confocal analysis of fluorescent MSN

The day prior to the experiment, HCT-116 cells were seeded onto bottom glass dishes (World Precision Instrument, Stevenage, UK) at a density of 10^6 cells cm^{-2}. On the day of the experiment, cells were washed once and incubated in 1 mL red-free medium containing fluorescent labeled nanoparticles at a concentration of 20 μg mL^{-1} for 6 h. Thirty minutes before the end of incubation, cells were loaded with 5 μg mL^{-1} Hoechst 33342 (Invitrogen, Cergy Pontoise, France) for nuclear staining.

For the lysosome labeling, 6 h before the end of the experiment, 50 nM lysotracker red DND-99 (Invitrogen) was added to phenol red-free DMEM. For endosome labeling, 20 min before the end of the experiment, 35 mg mL^{-1} transferrin (Invitrogen) were added to the culture medium. Before visualization, cells were washed gently with phenol red-free DMEM. Cells were then scanned with a LSM 5 LIVE confocal laser scanning microscope (Carl Zeiss, Le Pecq, France), with a slice depth (*Z* stack) of 0.67 μm (Vezenkov et al., 2010).

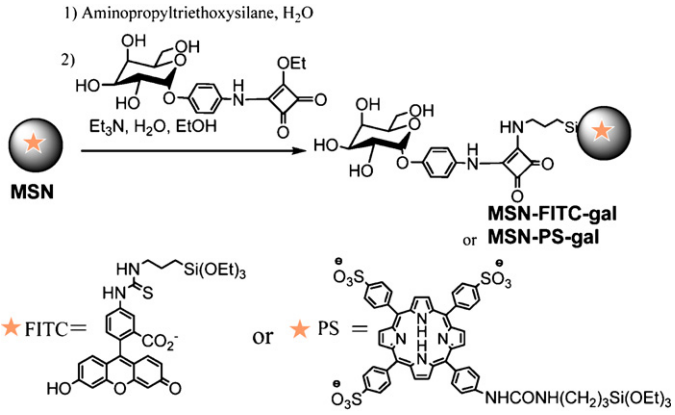

Fig. 1. Synthesis of functionalized MSN.

2.7. Statistical analysis

Statistical analysis was performed using the Student's *t* test to compare paired groups of data. A *p* value of <0.05 was considered to be statistically significant.

3. Results and discussion

3.1. Synthesis of the MSN

MSN encapsulating FITC (*MSN-FITC* and *MSN-FITC-NH_2*) were already synthesized and described (Hocine et al., 2010). MSN encapsulating water soluble photosensitizer (MSN-PS), were synthesized following our previously described methods (Brevet et al., 2009; Hocine et al., 2010). *p*-[*N*-(2-Ethoxy-3,4-dioxycyclobut-1-enyl)amino]phenyl-α-D-galactopyranoside was synthesized following an analogous pathway used for *p*-[*N*-(2-Ethoxy-3,4-dioxycyclobut-1-enyl)amino]phenyl-α-D-mannopyranoside (Sperling et al., 2006) and was grafted on the surface of the MSN through the APTS linker following our method already described with α-D-mannose (Brevet et al., 2009; Hocine et al., 2010). *MSN-FITC-gal* or *MSN-PS-gal* (Photosensitizer-galactose) were thus obtained (Fig. 1).

3.2. Confocal localization of fluorescent MSN in living cells

The cell distributions of *MSN-FITC* and *MSN-FITC-gal* were then studied after 6 h of incubation at 37 °C with living HCT-116 cancer cells.

MSN-FITC-gal (Fig. 2B and D) were clearly more efficiently internalized in comparison with unfunctionalized *MSN-FITC* (Fig. 2A and C). The addition in culture medium of an excess of galactose inhibits the internalization of *MSN-FITC-gal* demonstrating that these MSN were captured by a specific endocytosis involving galactose receptors. To gain more insight into *MSN-FITC-gal* internalization, co-stainings were performed with other fluorescent markers for subcellular components such as nucleus, mitochondries, endoplasmic reticulum, endosomes and lysosomes. The merged images showed that *MSN-FITC-gal* were partially co-localized (in yellow) with the endosomal (Fig. 2D) and the lysosomal (Fig. 2B) marker.

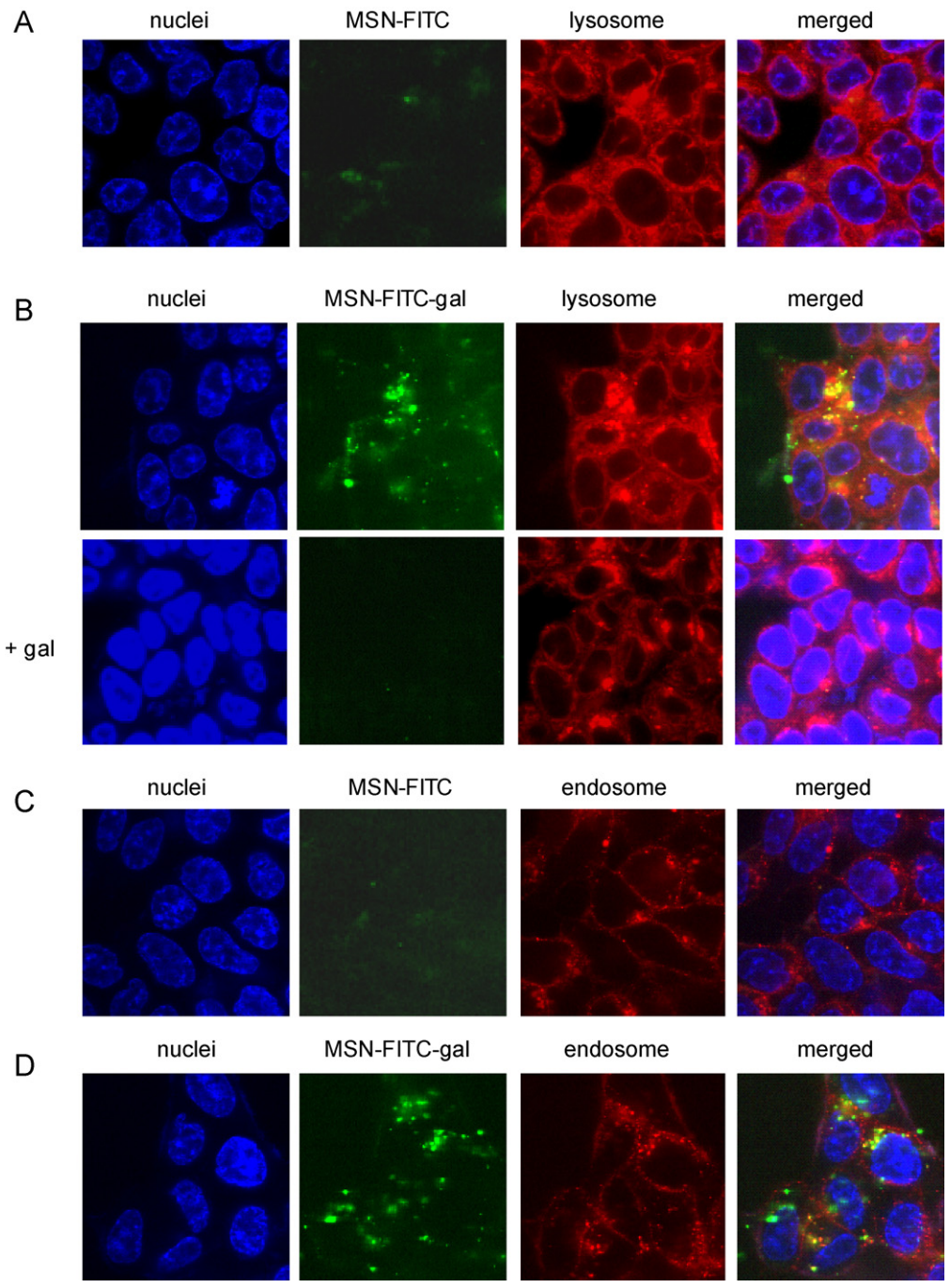

Fig. 2. Confocal microscopy images of living HCT-116 colorectal cancer cells, incubated for 6 h at 37 °C, with *MSN-FITC* (A and C) or *MSN-FITC-gal* (B and D), in presence or absence of 10 mM galactose (+ gal) (B). Merged pictures demonstrated the co-localization (yellow) of FITC-nanoparticles (green) with lysosomal or endosomal markers (red). Images are representative of at least 3 independent experiments. (For interpretation of the references to color in this figure legend and in text, the reader is referred to the web version of this article.)

In addition, no co-localization of *MSN-FITC-gal* was observed with mitochondrial or endoplasmic reticulum markers (data not shown). Altogether, these data indicate that the galactose functionalization significantly increases the cellular uptake of MSN through a specific endocytosis pathway leading to their sequentially accumulation in endosomal and lysosomal compartments.

3.3. Drug delivery

The pores of *MSN-PS-gal* were loaded with camptothecin following the method originally developed by Zink and Tamanoi (Lu et al., 2007b) to lead to *MSN-PS-CPT*. To study the cytotoxicity induced by *MSN-PS-gal-CPT*, HCT116 cells were treated with MSN at 20 $\mu g\ mL^{-1}$ and cell viability was monitored by using MTT assay to measure mitochondrial enzyme activity. Results showed that the cytotoxic effect increased up to 40% according to the incubation time with *MSN-PS-gal-CPT* (Fig. 3). These results confirmed the previous studies of Zink, Tamanoi and Nel (Liong et al., 2008; Lu et al., 2007b) who showed the potential of MSN for drug delivery with poorly water-soluble drugs.

Then, the same experiment was also performed on human MDA-MB-231 breast cancer cell line. Equivalent results were obtained

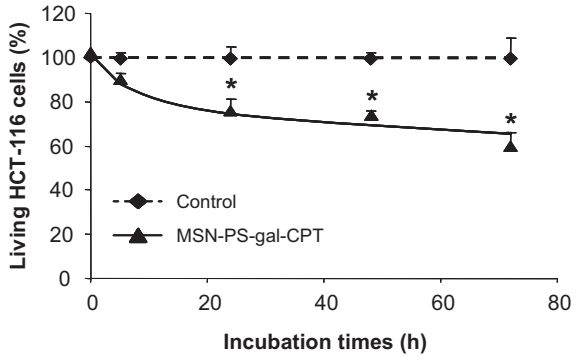

Fig. 3. Cytotoxic effect of MSN-camptothecin on human colorectal cancer cells. HCT-116 cells were incubated with *MSN-PS-gal-CPT* for 10 min, 5 h, 24 h, 48 h and 72 h. After incubation, medium was removed and cells were allowed to grow for 2 days. The level of living cells was measured and expressed as the percent of control cells. Data are mean ± SD of 3 independent experiments. $^{*}p < 0.05$ statistically different from control.

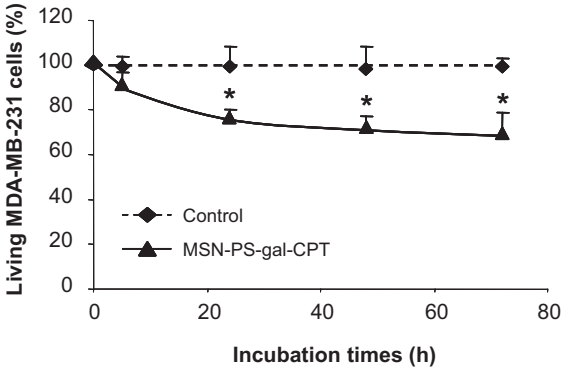

Fig. 4. Cytotoxic effect of MSN-PS-gal-CPT on human breast cancer cells. MDA-MB-231 cells were incubated with *MSN-PS-gal-CPT* for 10 min, 5 h, 24 h, 48 h and 72 h. After incubation, medium was removed and cells were allowed to grow for 2 days. The level of living cells was measured and expressed as the percent of control cells. Data are mean ± SD of 3 independent experiments. $^{*}p < 0.05$ statistically different from control.

(Fig. 4) demonstrating the significant cytotoxic effect of MSN encapsulating camptothecin and functionalized with galactose.

3.4. PDT and drug delivery

We next examined MSN combining drug delivery and PDT. Cells were treated with photo-activable nanoparticles functionalized with galactose and containing camptothecin (*MSN-PS-gal-CPT*) or not (*MSN-PS-gal*). For this experiment, HCT-116 cells were incubated for 24 h with 20 μg mL^{-1} MSN. After a change to a fresh culture medium, cells were irradiated for 40 min (630–680 nm; 6 mW cm^{-2}). A MTT assay was performed two days after irradiation to assess the cytotoxicity of MSN. We have first verified that 20 μg mL^{-1} *MSN-PS-gal* (without camptothecin) were not cytotoxic in the dark and that irradiation alone was not toxic for all tested cells (data not shown).

As shown in Fig. 5A, MSN with the photosensitizer *MSN-PS-gal* induced 44% HCT-116 cell death whereas treatment with MSN containing the photosensitizer and camptothecin *MSN-PS-gal-CPT* induced 83% cell death. In addition, equivalent results (79% versus 43% cells death with *MSN-PS-gal-CPT* and *MSN-PS-gal* respectively) were obtained on MDA-MB-231 cells (Fig. 5B). Interestingly, the irradiation appeared active at 24 h, when the cell delivery of the drug was already completed as observed in the time course of drug action (Figs. 3 and 4). This indicated that both therapies are successive and that toxicity due to irradiation was complementary to drug effect and could affected drug-resistant cells. The efficiency of *MSN-PS-gal-CPT* was also tested on pancreatic cancer cells such as Capan-1.

Results reported in Fig. 6A showed that without irradiation, *MSN-PS-gal-CPT* induced 38% cell death whereas *MSN-PS-gal* (MSN-PS) are not toxic. By contrast, Fig. 6B showed that, after irradiation at 650 nm, *MSN-PS-gal* induced 45% cell death whereas *MSN-PS-gal-CPT* induced 100% cell death in accordance with results already obtained on HCT-116 and MDA-MB-231 cells (Fig. 5). Taken together these data demonstrated that tri-functional *MSN-PS-gal-CPT* induced 79–100% cell death of three cancer cell lines, selected for their high invasive and metastatic potentials. The synergistic use of drug delivery and PDT with the same MSN may represent an alternative strategy in the context of poorly responsive tumors to current therapies. Further studies are required to define the mechanism leading to this synergistic action into the cells.

4. Conclusion

It was established that cancer cells have a high affinity for glycosylated ligands (Peng et al., 2007). We have recently demonstrated that a mannose targeting of MSN for PDT induced a higher

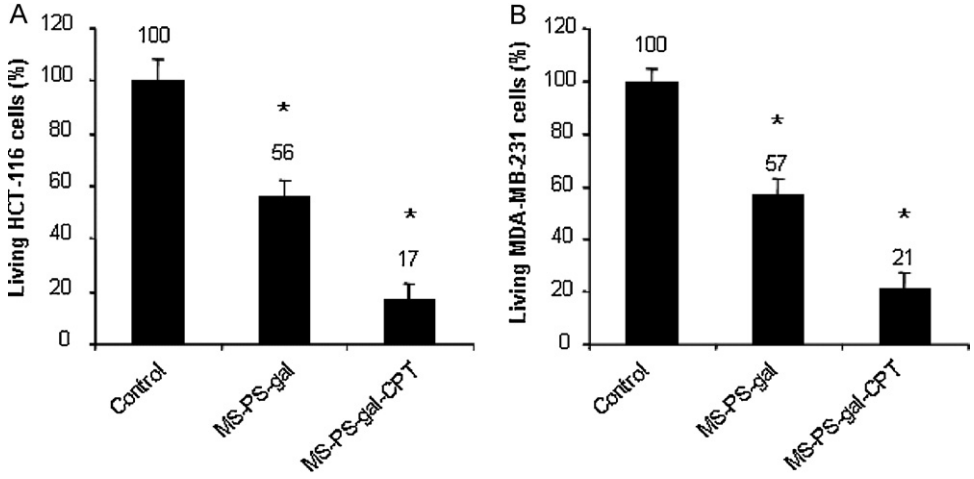

Fig. 5. Additional effect of PDT and drug delivery on cancer cells. HCT-116 (A) or MDA-MB-231 (B) cells were incubated or not (control) for 24 h with 20 μg mL^{-1} of *MSN-PS-gal* or *MSN-PS-gal-CPT*, then rinsed, maintained in fresh culture medium and submitted to laser irradiation (14 J cm^{-2}). Cells were allowed to grow for 2 days. Data are mean ± SD of 3 independent experiments. $^{*}p < 0.05$ statistically different from control.

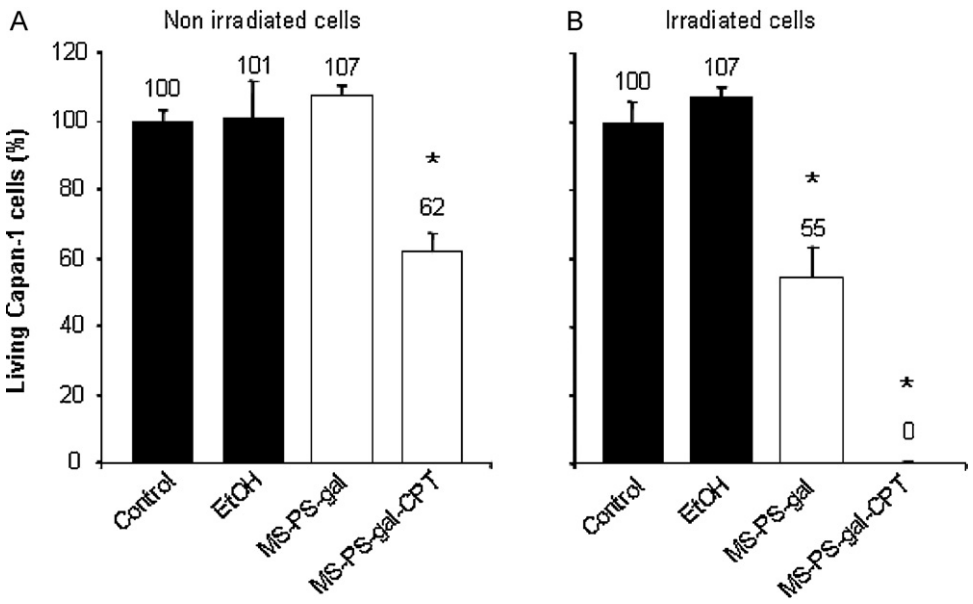

Fig. 6. Dual effect of MSN-CPT-PS on pancreatic cancer cells. Capan-1 cells were incubated or not (Control, EtOH) for 24 h with 20 μg mL^{-1} of *MSN-PS-gal* or *MSN-PS-gal-CPT*, then rinsed, maintained in fresh culture medium and submitted (B) or not (A) to laser irradiation (14 J cm^{-2}). Cells were allowed to grow for 2 days. Data are mean ± SD of 3 independent experiments. *$p < 0.05$ statistically different from control.

cytotoxicity of cancer cells than unfunctionalized ones (Brevet et al., 2009). In the present work, we demonstrated that galactose functionalization is also an efficient targeting of MSN to cancer cells. Through a specific galactose binding, nanoparticles are internalized and routed by the endocytic transport pathway from the plasma membrane to endosomes and finally to lysosomes.

Importantly, this work is the first evidence of a synergic anticancer effect of 2 active principles such as a photosensitizer (porphyrin) and a drug (camptothecin) in a same lectin-targeted MSN. These data provide the proof of principle that the use of two different mechanisms of drug action leads very efficiently to cancer cell death with the same nano-object.

Acknowledgements

Financial support by ANR PNANO. 07-102, *ARC n° SFI1201906*, and the non-profit organization Rétinostop (http://www.retinostop.org) is gratefully acknowledged. We thank Prof F. Tamanoi for discussions and Mr. M. Gleizes for technical assistance in cell biology experiments.

References

Brevet, D., Gary-Bobo, M., Raehm, L., Richeter, S., Hocine, O., Amro, K., Loock, B., Couleaud, P., Frochot, C., Morere, A., Maillard, P., Garcia, M., Durand, J.O., 2009. Mannose-targeted mesoporous silica nanoparticles for photodynamic therapy. Chem. Commun., 1475–1477.

Cauda, V., Engelke, H., Sauer, A., Arcizet, D., Brauchle, C., Radler, J., Bein, T., 2010. Colchicine-loaded lipid bilayer-coated 50 nm mesoporous nanoparticles efficiently induce microtubule depolymerization upon cell uptake. Nano Lett. 10, 2484–2492.

Chen, A.M., Zhang, M., Wei, D.G., Stueber, D., Taratula, O., Minko, T., He, H.X., 2009. Co-delivery of doxorubicin and bcl-2 sirna by mesoporous silica nanoparticles enhances the efficacy of chemotherapy in multidrug-resistant cancer cells. Small 5, 2673–2677.

Cheng, S.-H., Lee, C.-H., Chen, M.-C., Souris, J.S., Tseng, F.-G., Yang, C.-S., Mou, C.-Y., Chen, C.-T., Lo, L.-W., 2010. Tri-functionalization of mesoporous silica nanoparticles for comprehensive cancer theranostics – the trio of imaging, targeting and therapy. J. Mater. Chem. 20, 6149–6157.

Cheng, S.-H., Lee, C.-H., Yang, C.-S., Tseng, F.-G., Mou, C.-Y., Lo, L.-W., 2009. Mesoporous silica nanoparticles functionalized with an oxygen-sensing probe for cell photodynamic therapy: potential cancer theranostics. J. Mater. Chem. 19, 1252–1257.

Coti, K.K., Belowich, M.E., Liong, M., Ambrogio, M.W., Lau, Y.A., Khatib, H.A., Zink, J.I., Khashab, N.M., Stoddart, J.F., 2009. Mechanised nanoparticles for drug delivery. Nanoscale 1, 16–39.

Couleaud, P., Morosini, V., Frochot, C., Richeter, S., Raehm, L., Durand, J.O., 2010. Silica-based nanoparticles for photodynamic therapy applications. Nanoscale 2, 1083–1095.

Gallo, R.C., Whangpen, J., Adamson, R.H., 1971. Studies on antitumor activity, mechanism of action, and cell cycle effects of camptothecin. J. Nat. Cancer Inst. 46, 789–795.

Gary-Bobo, M., Mir, Y., Rouxel, C., Brevet, D., Basile, I., Maynadier, M., Vaillant, O., Mongin, O., Blanchard-Desce, M., Morere, A., Garcia, M., Durand, J.-O., Raehm, L., 2011. Mannose-functionalized mesoporous silica nanoparticles for efficient two-photon photodynamic therapy of solid tumors. Angew. Chem. Int. Ed. 50, 11425–11429.

Gottlieb, J.A., Guarino, A.M., Call, J.B., Oliverio, V.T., Block, J.B., 1970. Preliminary pharmacologic and clinical evaluation of camptothecin sodium (nsc-100880). Cancer Chemother. Rep. Part 1 54, 461–470.

Guo, H., Qian, H., Idris, N.M., Zhang, Y., 2010. Singlet oxygen-induced apoptosis of cancer cells using upconversion fluorescent nanoparticles as a carrier of photosensitizer. Nanomedicine 6, 486–495.

Hocine, O., Gary-Bobo, M., Brevet, D., Maynadier, M., Fontanel, S., Raehm, L., Richeter, S., Loock, B., Couleaud, P., Frochot, C., Charnay, C., Derrien, G., Smaïhi, M., Sahmoune, A., Morère, A., Maillard, P., Garcia, M., Durand, J.-O., 2010. Silicalites and mesoporous silica nanoparticles for photodynamic therapy. Int. J. Pharm. 402, 221–230.

Hsiao, J.K., Tsai, C.P., Chung, T.H., Hung, Y., Yao, M., Liu, H.M., Mou, C.Y., Yang, C.S., Chen, Y.C., Huang, D.M., 2008. Mesoporous silica nanoparticles as a delivery system of gadolinium for effective human stem cell tracking. Small 4, 1445–1452.

Kim, H.J., Shin, K.J., Han, M.K., An, K., Lee, J.K., Honma, I., Kim, H., 2009. One-pot synthesis of multifunctional mesoporous silica nanoparticle incorporated with zinc(ii) phthalocyanine and iron oxide. Scripta Mater. 61, 1137–1140.

Lebold, T., Jung, C., Michaelis, J., Brauchle, C., 2009. Nanostructured silica materials as drug-delivery systems for doxorubicin: single molecule and cellular studies. Nano Lett. 9, 2877–2883.

Lebret, V., Raehm, L., Durand, J.O., Smaihi, M., Werts, M.H.V., Blanchard-Desce, M., Methy-Gonnod, D., Dubernet, C., 2008. Surface functionalization of two-photon dye-doped mesoporous silica nanoparticles with folic acid: cytotoxicity studies with hela and mcf-7 cancer cells. J. Sol-Gel Sci. Technol. 48, 32–39.

Lebret, V., Raehm, L., Durand, J.O., Smaihi, M., Werts, M.H.V., Blanchard-Desce, M., Methy-Gonnod, D., Dubernet, C., 2010. Folic acid-targeted mesoporous silica nanoparticles for two-photon fluorescence. J. Biomed. Nanotechnol. 6, 176–180.

Lee, C.H., Cheng, S.H., Wang, Y.J., Chen, Y.C., Chen, N.T., Souris, J., Chen, C.T., Mou, C.Y., Yang, C.S., Lo, L.W., 2009. Near-infrared mesoporous silica nanoparticles for optical imaging: characterization and in vivo biodistribution. Adv. Func. Mater. 19, 215–222.

Lee, J.E., Lee, N., Kim, H., Kim, J., Choi, S.H., Kim, J.H., Kim, T., Song, I.C., Park, S.P., Moon, W.K., Hyeon, T., 2010. Uniform mesoporous dye-doped silica nanoparticles decorated with multiple magnetite nanocrystals for simultaneous enhanced magnetic resonance imaging, fluorescence imaging, and drug delivery. J. Am. Chem. Soc. 132, 552–557.

Li, L.H., Bhuyan, B.K., Fraser, T.J., Olin, E.J., 1972. Action of camptothecin on mammalian-cells in culture. Cancer Res. 32, 2643–2650.
Lin, Q.N., Huang, Q., Li, C.Y., Bao, C.Y., Liu, Z.Z., Li, F.Y., Zhu, L.Y., 2010. Anticancer drug release from a mesoporous silica based nanophotocage regulated by either a one- or two-photon process. J. Am. Chem. Soc. 132, 10645–10647.
Lin, Y.-S., Tsai, C.-P., Huang, H.-Y., Kuo, C.-T., Hung, Y., Huang, D.-M., Chen, Y.-C., Mou, C.-Y., 2005. Well-ordered mesoporous silica nanoparticles as cell markers. Chem. Mater. 17, 4570–4573.
Liong, M., Angelos, S., Choi, E., Patel, K., Stoddart, J.F., Zink, J.I., 2009. Mesostructured multifunctional nanoparticles for imaging and drug delivery. J. Mater. Chem. 19, 6251–6257.
Liong, M., Lu, J., Kovochich, M., Xia, T., Ruehm, S.G., Nel, A.E., Tamanoi, F., Zink, J.I., 2008. Multifunctional inorganic nanoparticles for imaging, targeting, and drug delivery. ACS Nano 2, 889–896.
Liu, H.M., Wu, S.H., Lu, C.W., Yao, M., Hsiao, J.K., Hung, Y., Lin, Y.S., Mou, C.Y., Yang, C.S., Huang, D.M., Chen, Y.C., 2008. Mesoporous silica nanoparticles improve magnetic labeling efficiency in human stem cells. Small 4, 619–626.
Lu, J., Choi, E., Tamanoi, F., Zink, J.I., 2008. Light-activated nanoimpeller-controlled drug release in cancer cells. Small 4, 421–426.
Lu, J., Liong, M., Li, Z., Zink, J.I., Tamanoi, F., 2010. Biocompatibility, biodistribution, and drug-delivery efficiency of mesoporous silica nanoparticles for cancer therapy in animals. Small 6, 1794–1805.
Lu, J., Liong, M., Sherman, S., Xia, T., Kovochich, M., Nel, A.E., Zink, J.I., Tamanoi, F., 2007a. Mesoporous silica nanoparticles for cancer therapy: energy-dependent cellular uptake and delivery of paclitaxel to cancer cells. Nanobiotechnology 3, 89–95.
Lu, J., Liong, M., Zink, J.I., Tamanoi, F., 2007b. Mesoporous silica nanoparticles as a delivery system for hydrophobic anticancer drugs. Small 3, 1341–1346.
Meng, H.A., Liong, M., Xia, T.A., Li, Z.X., Ji, Z.X., Zink, J.I., Nel, A.E., 2010. Engineered design of mesoporous silica nanoparticles to deliver doxorubicin and *p*-glycoprotein sirna to overcome drug resistance in a cancer cell line. ACS Nano 4, 4539–4550.
Mortera, R., Vivero-Escoto, J., Slowing, I.I., Garrone, E., Onida, B., Lin, V.S.Y., 2009. Cell-induced intracellular controlled release of membrane impermeable cysteine from a mesoporous silica nanoparticle-based drug delivery system. Chem. Commun., 3219–3221.
Na, H.B., Hyeon, T., 2009. Nanostructured t1 mri contrast agents. J. Mater. Chem. 19, 6267–6273.
Peng, J., Wang, K., Tan, W., He, X., He, C., Wu, P., Liu, F., 2007. Identification of live liver cancer cells in a mixed cell system using galactose-conjugated fluorescent nanoparticles. Talanta 71, 833–840.
Rosenholm, J., Sahlgren, C., Linden, M., 2010a. Cancer-cell targeting and cell-specific delivery by mesoporous silica nanoparticles. J. Mater. Chem. 20, 2707–2713.
Rosenholm, J.M., Meinander, A., Peulhu, E., Niemi, R., Eriksson, J.E., Sahlgren, C., Linden, M., 2009. Targeting of porous hybrid silica nanoparticles to cancer cells. ACS Nano 3, 197–206.
Rosenholm, J.M., Peuhu, E., Bate-Eya, L.T., Eriksson, J.E., Sahlgren, C., Linden, M., 2010b. Cancer-cell-specific induction of apoptosis using mesoporous silica nanoparticles as drug-delivery vectors. Small 6, 1234–1241.
Rosenholm, J.M., Sahlgren, C., Linden, M., 2010c. Towards multifunctional, targeted drug delivery systems using mesoporous silica nanoparticles – opportunities and challenges. Nanoscale 2, 1870–1883.
Slowing, I.I., Trewyn, B.G., Giri, S., Lin, V.S.Y., 2007. Mesoporous silica nanoparticles for drug delivery and biosensing applications. Adv. Func. Mater. 17, 1225–1236.
Slowing, I.I., Vivero-Escoto, J.L., Trewyn, B.G., Lin, V.S.Y., 2010. Mesoporous silica nanoparticles: structural design and applications. J. Mater. Chem. 20, 7924–7937.
Slowing, I.I., Vivero-Escoto, J.L., Wu, C.-W., Lin, V.S.Y., 2008. Mesoporous silica nanoparticles as controlled release drug delivery and gene transfection carriers. Adv. Drug Deliv. Rev. 60, 1278–1288.
Sperling, O., Fuchs, A., Lindhorst, T.K., 2006. Evaluation of the carbohydrate recognition domain of the bacterial adhesin fimh: design, synthesis and binding properties of mannoside ligands. Org. Biomol. Chem. 4, 3913–3922.
Taylor, K.M.L., Kim, J.S., Rieter, W.J., An, H., Lin, W.L., Lin, W.B., 2008. Mesoporous silica nanospheres as highly efficient mri contrast agents. J. Am. Chem. Soc. 130, 2154–2155.
Trewyn, B.G., Giri, S., Slowing, I.I., Lin, V.S.Y., 2007a. Mesoporous silica nanoparticle based controlled release, drug delivery, and biosensor systems. Chem. Commun., 3236–3245.
Trewyn, B.G., Slowing, I.I., Giri, S., Chen, H.-T., Lin, V.S.Y., 2007b. Synthesis and functionalization of a mesoporous silica nanoparticle based on the sol-gel process and applications in controlled release. Acc. Chem. Res. 40, 846–853.
Tsai, C.P., Chen, C.Y., Hung, Y., Chang, F.H., Mou, C.Y., 2009. Monoclonal antibody-functionalized mesoporous silica nanoparticles (msn) for selective targeting breast cancer cells. J. Mater. Chem. 19, 5737–5743.
Tu, H.-L., Lin, Y.-S., Hung, Y., Lo, L.-W., Chen, Y.-F., Mou, C.-Y., 2009. In vitro studies of functionalized mesoporous silica nanoparticles for photodynamic therapy. Adv. Mater. 21, 172–174.
Vezenkov, L.L., Maynadier, M., Hernandez, J.-F., Averlant-Petit, M.-C., Fabre, O., Benedetti, E., Garcia, M., Martinez, J., Amblard, M., 2010. Noncationic dipeptide mimic oligomers as cell penetrating nonpeptides (cpnp). Bioconjugate Chem. 21, 1850–1854.
Vivero-Escoto, J.L., Slowing, I.I., Wu, C.W., Lin, V.S.Y., 2009. Photoinduced intracellular controlled release drug delivery in human cells by gold-capped mesoporous silica nanosphere. J. Am. Chem. Soc. 131, 3462–3463.
Vivero-Escoto, J.L., Slowing, I.I., Trewyn, B.G., Lin, V.S.Y., 2010. Mesoporous silica nanoparticles for intracellular controlled drug delivery. Small 6, 1952–1967.
Wu, S.-H., Lin, Y.-S., Hung, Y., Chou, Y.-H., Chang, C., Mou, C.-Y., 2007. Multifunctional mesoporous silica nanoparticles as dual-mode imaging probes. Stud. Surf. Sci. Catal. 170B, 1804–1810.
Yang, Y., Song, W.X., Wang, A.H., Zhu, P.L., Fei, J.B., Li, J.B., 2010. Lipid coated mesoporous silica nanoparticles as photosensitive drug carriers. Phys. Chem. Chem. Phys. 12, 4418–4422.
Zhang, Y., Zhi, Z., Jiang, T., Zhang, J., Wang, Z., Wang, S., 2010. Spherical mesoporous silica nanoparticles for loading and release of the poorly water-soluble drug telmisartan. J. Control. Release 145, 257–263.